



Chemical–mechanical coupling observed for depleted oil reservoirs subjected to long-term CO₂-exposure – A case study of the Werkendam natural CO₂ analogue field



Suzanne Hangx^{a,b,*}, Elisenda Bakker^b, Pieter Bertier^c, Georg Nover^d, Andreas Busch^a

^a Shell Global Solutions, Kesslerpark 1, 2288 GS Rijswijk, The Netherlands

^b Department of Earth Sciences, Utrecht University, Budapestlaan 4, 3584 CD Utrecht, The Netherlands

^c Clay and Interface Mineralogy, RWTH Aachen University, Intzestrasse 1, 52056 Aachen, Germany

^d Steinmann Institute, Bonn University, Poppelsdorfer Schloss, 53115 Bonn, Germany

ARTICLE INFO

Article history:

Received 27 December 2014

Received in revised form 5 July 2015

Accepted 20 July 2015

Available online 6 August 2015

Editor: J. Brodholt

Keywords:

CO₂/brine/rock interaction
storage integrity
rock mechanics
natural CO₂ analogue
bitumen coatings

ABSTRACT

Geological storage of CO₂ is one of the most promising technologies to rapidly reduce anthropogenic emissions of carbon dioxide. In order to ensure storage integrity, it is important to understand the effect of long-term CO₂/brine/rock interactions on the mechanical behaviour of a storage complex. As most of these reactions are too slow to reproduce on laboratory timescales, we studied a natural CO₂ analogue reservoir (the Röt Fringe Sandstone, Werkendam field, the Netherlands; 125–135 Ma of CO₂-exposure) and its unreacted counterpart. We focused on CO₂-induced mineralogical and porosity-permeability changes, and their effect on mechanical behaviour of both intact rock and simulated fault gouge. Overall, CO₂-exposure did not lead to drastic mineralogical changes. The CO₂-exposed material shows a stronger dependence of permeability on porosity, which is attributed to differences in diagenesis (closed-system diagenesis and hydrocarbon emplacement) taking place before CO₂ charging. The limited extent of reaction was in part the result of bitumen coatings protecting specific mineral phases from reaction. In local, mm-sized zones displaying significant anhydrite cement dissolution, enhanced porosity was observed. For most of the reservoir the long-term mechanical behaviour after CO₂-exposure could be described by the behaviour of the unreacted sandstone, while these more ‘porous’ zones had a lower rock strength. In addition, CO₂-exposure did not affect the fault friction behaviour, and slip is expected to result in stable sliding. Simple stress path calculations predict that reservoir failure due to depletion and injection is unlikely, even for the ‘porous’ zones, nor will fault reactivation occur for realistic injection scenarios.

© 2015 Elsevier B.V. All rights reserved.

1. Introduction

The Intergovernmental Panel on Climate Change has shown that atmospheric CO₂ levels have risen from pre-industrial levels of 280 ppm to 387 ppm in 2005, with current growth rates of ~1.9 ppm/yr (IPCC, 2007). A recently published report by the International Energy Agency (IEA, 2013) shows an increase in global carbon emissions in 2012 by 1.4% compared to 2011 – the highest value reported to date. Carbon capture and storage (CCS) is potentially able to reduce these emissions on a short to medium time scale, with global storage capacities ranging from 100's to 1000's of gigatonnes (Dooley et al., 2006). Currently, CCS projects

in the operate or execute phase amount to annual CO₂ emissions reductions of ~8 Mt, corresponding to only ~0.2% of the globally emitted ~37 Gt in 2014 (Global Carbon Project, 2015). Lack of public acceptance of CCS technology is an important reason for the low injection volumes. Key concerns are whether CCS is a safe technology and if the stored CO₂ will remain in the subsurface for >10,000 yr, i.e. is storage integrity maintained?

After injection, supercritical CO₂ is present below a sealing barrier, commonly referred to as structural trapping. Therefore, maintaining caprock integrity is important to prevent structurally trapped CO₂ from leaving the reservoir. In order to better understand storage integrity and how CO₂/brine/rock interactions may affect CO₂ flow pathways and/or mechanical rock parameters, the study of natural CO₂ analogue systems is necessary (Bickle et al., 2013; Kampman et al., 2014). In such fields, CO₂ has been present in the subsurface for over thousands of years (e.g. see

* Corresponding author at: Department of Earth Sciences, Utrecht University, Budapestlaan 4, 3584 CD Utrecht, The Netherlands.

E-mail address: s.j.t.hangx@uu.nl (S. Hangx).

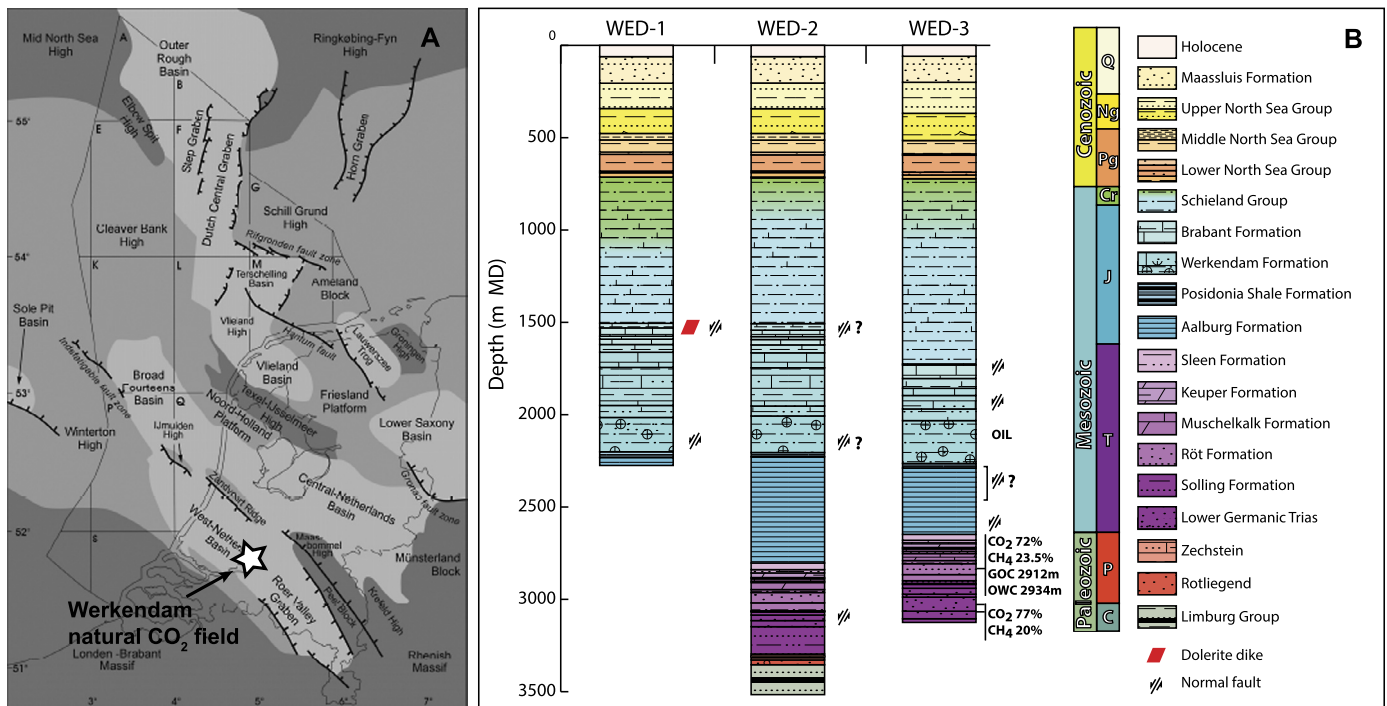


Fig. 1. (A) Major structural elements of the geology of the Netherlands and location of the Werkendam natural CO₂ field (adapted from Geluk, 2005). (B) Lithostratigraphy of the Werkendam wells. Note that for well WED-3, GOC signifies the gas-oil contact and OWC the oil-water contact. (For interpretation of the colours in this figure, the reader is referred to the web version of this article.)

Burnside et al., 2013; Watson et al., 2004). Studies investigating CO₂/brine/rock interactions occurring in natural CO₂-rich siliciclastic reservoirs showed that the majority of reactions involve dissolution of feldspars and micas, and the precipitation of clays (e.g. illite, kaolinite) and carbonates (Baines and Worden, 2004; May, 2005; Moore et al., 2005; Pearce et al., 2004; Watson et al., 2004). Though CO₂ mineralisation in the form of carbonate minerals is argued to be a major sink for CO₂, detailed geochemical studies found that carbonate precipitation from CO₂-rich fluids is rather limited (Gilfillan et al., 2009). This means that most of the injected CO₂ will remain present as a liquid or supercritical phase below the sealing formation. In natural CO₂ fields where leakage occurred, measured leakage rates varied from ~ 40 to $2 \cdot 10^{-5}$ t CO₂ m²/yr (Burnside et al., 2013; Streit and Watson, 2004), depending on the leakage mechanism (i.e. fault leakage or diffusion-controlled leakage). Furthermore, recent work has demonstrated the importance of geomechanical studies in the overall evaluation of potential reservoirs considered for CCS (Verdon et al., 2013). Detailed laboratory studies on the changes of rock mechanical parameters due to CO₂/water/rock interactions are few, as reaction time scales often exceed those suitable for laboratory experimentation (for sandstones see Hangx et al., 2013, 2010a; Marbler et al., 2013; Mikhaltsevitch et al., 2014). Studies of natural CO₂ fields can aid in understanding long-term chemical-mechanical behaviour and improve the confidence in the mechanical stability of caprocks and reservoirs (e.g. see Major et al., 2014; Trippetta et al., 2013).

In this study we focus on the onshore Werkendam natural CO₂ analogue located in the West Netherlands Basin, near the city of Rotterdam. The Nederlandse Aardolie Maatschappij (NAM) has been, and still is, exploring for oil and gas in this basin and discovered a reservoir with an underdeveloped gas cap and an underdeveloped oil rim in the Upper Bunter formation. The gas cap, situated at a depth of ~ 3000 m consists of some 72% CO₂. Adjacent to this reservoir, the same formation was encountered without any gas and oil-bearing horizons. The CO₂ is considered to originate from igneous activity related to rifting events in Early Cretaceous

times (~ 125 – 135 Ma). The Werkendam case provides an excellent opportunity to study the long-term effect of CO₂ on sandstone diagenesis. In the following we will address these changes in terms of reservoir diagenesis, flow properties, rock mechanics, as well as consequences for the long-term fate of CO₂ in the subsurface.

2. Geological setting of the West-Netherlands Basin

The Werkendam natural CO₂ analogue field is situated near the city of Werkendam, in the West-Netherlands Basin (WNB), southwest Netherlands (~ 20 km southeast of Rotterdam – see Fig. 1A). Drilling initiated with a vertical well Werkendam-1 in 1958 (WED1, 2258 m total vertical depth (TVD)), followed by a second vertical well in 1965 on the same site (WED2, 3516 m TVD). Though WED1 produced hydrocarbons, WED2 did not. Therefore a deviated well (WED3, 3125 m TVD, 1991) was drilled from about the same surface position as WED1 and WED2.

The basin underwent two main tectonic phases, (1) Jurassic–Early Cretaceous rifting, and (2) Late Cretaceous–Early Cenozoic uplift (Racero-Baena and Drake, 1996), leading to the formation of a major fault system near the drill location, consisting of two sets of roughly parallel striking normal faults, dipping in different directions. The formation of interest consists of Röt Fringe Sandstone, which is overlain by Röt claystones and evaporites.

During rifting the underlying Carboniferous source rocks were brought within the oil/gas maturation window. Hydrocarbon migration and emplacement was inferred to have taken place during the Jurassic rifting phase. At present the reservoir contains a thin oil rim (22 m) and a gas leg of about 105 m. Later during the rifting stage, post-dating the hydrocarbon charging, CO₂ emplacement of the Röt Fringe formation most likely occurred along the SW-dipping faults, resulting from Late Kimmerian magmatic activity, some 125–135 Ma ago. Current day, the gas present in the Werkendam field contains about 72% CO₂ and 23.5% CH₄.

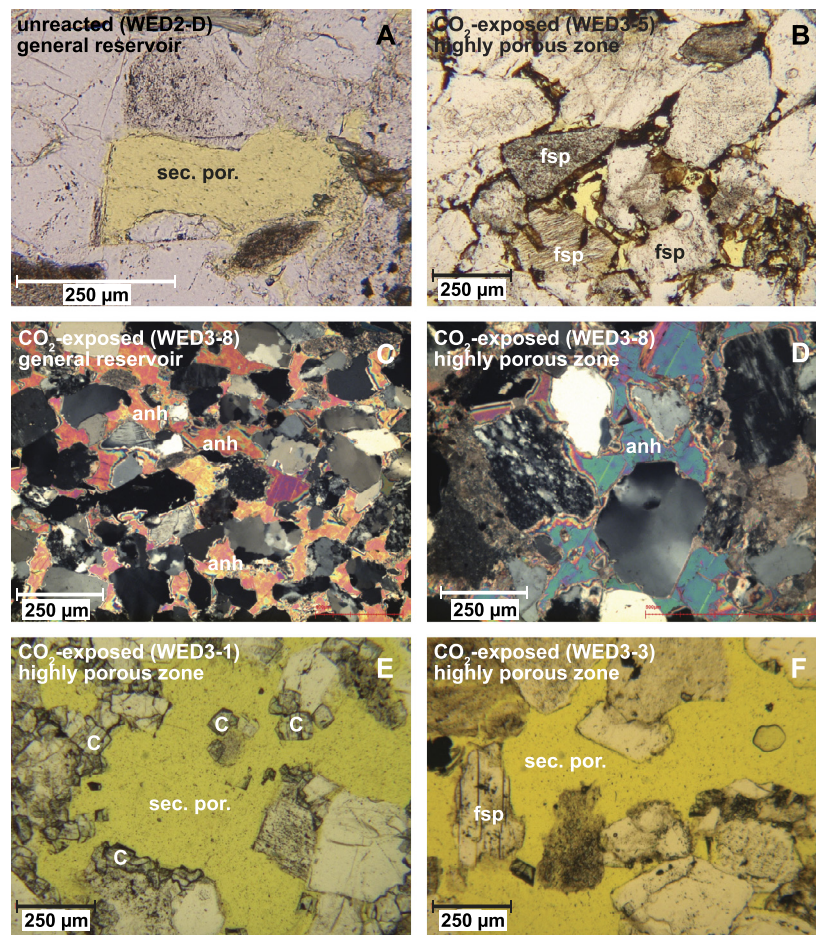


Fig. 2. Optical micrographs of representative thin section illustrating the petrography of the Werkendam reservoir sandstones. (A) WED2-D (2977.75 m): Open secondary pore (sec. por., filled with yellow dyed epoxy resin) resulting from feldspar alteration. (B) WED3-5 (2829.35 m): Relatively unaltered feldspar grains in a bitumen-coated sample of the Werkendam 3 well. (C) WED3-8 (2834.45 m): Pre-compactional, grain-replacive anhydrite cement, filling abundant primary porosity. (D) WED3-7 (2833.8 m): Detail of pre-compactional anhydrite cement, replacing framework grains. (E) WED3-1 (2821.6 m): Large anhydrite cement dissolution porosity in a sample of the Werkendam 3 well. Early dolomite cement (C) was not affected by this dissolution event. (F) WED3-3 (2824.85 m): Large anhydrite cement dissolution porosity in a sample of the Werkendam 3 well. Feldspar grains (fsp) were not affected by this dissolution event. (For interpretation of the references to colour in this figure legend, the reader is referred to the web version of this article.)

3. Starting material and experimental methods

Röt Fringe Sandstone sample material was obtained from core retrieved from the WED2 (unreacted, 2971–2993 m depth) and WED3 (CO₂-exposed, 2821–2846 m depth) wells (courtesy of NAM). **X-ray Diffraction Analysis (XRD)** was performed to derive bulk mineralogical compositions (see Section 1.1 in the Supplementary Material for details). Furthermore, representative thin sections of the starting material (see Fig. 2) were examined by **polarised light, UV and cathodoluminescence microscopy**. Prior to the mechanical experiments, **density, porosity and permeability** were measured on cylindrical plugs (25 mm diameter, 50–75 mm length), with square ground and polished ends.

Rock strength experiments were performed on these intact, cylindrical samples in axisymmetric compression, using two different triaxial machines (Hangx et al., 2013, 2010b), at room temperature under both dry (room humidity) and wet conditions. Strain rate is $\sim 10^{-5} \text{ s}^{-1}$, which is faster than generally observed in nature. However, since rock strength is near-independent of strain rate, this will not affect our measurements (Paterson and Wong, 2005). Wet experiments are done under drained conditions, employing artificial reservoir brine. The raw data are processed to yield differential stress ($\sigma_1 - \sigma_3$) (i.e. stress difference across the sample), axial strain e (i.e. axial shortening), and volumetric strain e_{vol} (i.e. volumetric change) versus time, while being accurately

corrected for apparatus distortion. Compressive stresses, compressive axial strains and dilatant volumetric strains (dilatation) are measured positive. The principal compressive stresses are denoted σ_i , with $\sigma_1 > \sigma_2 = \sigma_3 = P_c$. Accordingly, the effective principal stresses are denoted σ_i^{eff} , and are defined as $\sigma_i^{\text{eff}} = \sigma_i - P_p$. Peak strength is defined as the maximum differential stress $(\sigma_1 - \sigma_3)_{\text{max}}$ supported by a given sample and failure as the loss of strength of the material beyond the peak. Yield strength (σ_y) is the differential stress at which the differential stress versus axial strain curve deviates from linearity (Fredrich et al., 1989). The elastic parameters of individual samples, the apparent Young's modulus (E_a) and bulk modulus (K_a), are determined from the linear portion of the stress–axial strain and volumetric strain–axial strain curves respectively (Baud et al., 2000; Zoback and Byerlee, 1975) – for details see Section 1.2 and Fig. S2 in the Supplementary Material.

In addition, **direct-shear experiments** are performed to study the frictional behaviour of the material. Fault gouge material was simulated by crushing intact core (WED2, 2991.5 m depth; WED3, 2445.3 m depth) using a mortar and pestle, and sieving the material to a grain size of less than 35 μm . Velocity-stepping direct-shear experiments are conducted dry (room humidity), at room temperature and at different normal stresses, using a shear assembly within a triaxial apparatus (Samuelson and Spiers, 2012). The frictional behaviour of the simulated fault gouge is explained using the theory of rate and state friction (RSF), which states that a pos-

Table 1

Sample ID	Mineralogy													Petrophysics ^a				Geomechanics						
	Depth [m]	Depositional environment ^b	Quartz [mass-%]	Feldspar [mass-%]	Clay + Mica [mass-%]	Calcite [mass-%]	Dolomite [mass-%]	Siderite [mass-%]	Anhydrite [mass-%]	Gypsum [mass-%]	Barite [mass-%]	Hematite [mass-%]	Anatase [mass-%]	Density [g/cm ³]	Horizontal permeability [mD]	Vertical permeability [mD]	Horizontal porosity [%]	Vertical porosity [%]	Confining pressure P_c [MPa]	Pore fluid pressure P_p [MPa]	Yield stress σ_y [MPa]	Peak stress $(\sigma_1 - \sigma_3)_{max}$ [MPa]	Apparent Young's Modulus E_d [GPa]	Apparent bulk Modulus K_d [GPa]
<i>WED2: unreacted</i>																								
Wed2-A	2971.9	PL	31.43	8.86	48.93		7.97	0.99	0.12	0.14	0.05	1.52	0.00	2.729		0.01		1.58						
Wed2-B	2973.35	SF	57.27	3.93	19.53		16.28	1.47	1.25	0.00	0.00	0.00	0.26	2.747	0.09	0.04	5.43	5.07	0.5	0.1	59.5	61.1	8.2	9.5
Wed2-C green ^c	2974.0	PL	24.09	5.81	56.35		9.69	2.62	0.51	0.16	0.07	0.71	0.00	2.758	0.11	0.01	2.40	1.18						
Wed2-C red ^c	2974.1	PL	16.74	3.67	69.16		5.71	0.48	0.51	0.21	0.04	3.47	0.00											
Wed2-D	2977.75	BC	68.59	5.30	19.30		4.15	1.43	1.11	0.00	0.00	0.00	0.13	2.669	0.74	0.44	14.10	11.92						
Wed2-E	2979.25	BC	44.50	2.16	6.85		45.16	0.37	0.23	0.46	0.15	0.13	0.00	2.906	0.11	0.04	5.70	2.07						
Wed2-F	2984.1	BC	72.59	6.76	18.54		0.21	0.81	0.69	0.17	0.15	0.07	0.00	2.705	0.77	0.43	14.56	15.91						
Wed2-G	2989.9	BC	56.60	4.97	15.35		17.12	0.82	4.99	0.00	0.00	0.00	0.15	2.719	0.14	0.05	5.85	3.94	0.5	0.1	83.9	91.0	13.4	16.8
Wed2-M	2991.0																		2.0	-	133.6	152.7	20.8	n.a. ^e
Wed2-N	2991.0																		35.0	10.0	198.1	256.4	26.2	37.9
Wed2-K	2991.15																		25.0	-	182.2	221.7	26.8	23.1
Wed2-L	2991.15																		50.0	-	208.2	285.2	28.2	22.9
Wed2-J	2991.3																		5.0	-	112.3	127.6	21.0	19.4
Wed2-H fine ^c	2991.7	PL	11.77	4.05	73.65		5.22	0.00	0.29	0.14	0.03	4.79	0.00	2.716	0.26	0.07	3.52	1.05	0.5	0.1	80.5	81.4	11.3	14.0
Wed2-H coarse ^c	2991.8	SF	53.06	6.20	14.38		9.00	0.30	13.80	2.60	0.10	0.30	0.00											
Wed2-I	2992.9	SF	55.10	7.57	18.10		1.20	1.25	14.55	2.25	0.00	0.00	0.00	2.716	0.05	0.03	2.81	0.57	0.5	0.1	n.a. ^d	n.a. ^d	14.8	17.5
<i>WED3: CO₂-exposed</i>																								
Wed3-1	2821.6	BC	56.14	7.12	6.85	0.15	28.22	0.73	0.21	0.00	0.57	0.00		2.732	14.40	2.37	11.06	10.12						
Wed3-2	2824.3	PL	25.44	14.22	57.52	0.03	0.74	1.52	0.54	0.00	0.00	0.00		2.756	0.14	0.01	1.45							
Wed3-3	2824.85	BC	77.65	12.32	4.95	0.30	1.62	0.58	0.07	0.00	2.51	0.00		2.712	285.00	160.74	16.50	6.25	5.5	0.5	57.9	79.9	10.0	15.3
Wed3-4	2828.3	BC	67.64	13.74	14.94	0.43	2.11	0.57	0.25	0.00	0.30	0.00		2.679	62.00	4.15	13.67	13.68						
Wed3-5	2829.35	SF	72.43	20.00	4.01	0.00	1.91	0.83	0.03	0.00	0.80	0.00		2.634	38.00	15.43	15.48	13.78						
Wed3-18	2829.38																		5.0	-	78.9	92.9	15.1	24.8
Wed3-19	2829.38																		2.0	-	66.4	71.6	13.7	12.5
Wed3-20	2829.38																		25.0	-	132.1	162.6	20.2	32.0
Wed3-21	2829.41																		50.0	-	172.7	241.5	26.3	n.a. ^e
Wed3-6	2830.6	BC	40.55	13.59	18.41	0.00	26.96	0.08	0.32	0.00	0.10	0.00		2.658	1.06	0.42	5.45	8.16						
Wed3-16	2833.6																		2.0	-	68.8	74.0	10.6	n.a. ^e
Wed3-17	2833.6																		35.0	10.0	122.8	158.4	18.4	26.8
Wed3-7	2833.8	SF	53.61	12.94	14.80	0.00	6.73	0.65	9.12	1.07	1.08	0.00		2.708	0.35	0.08	4.60	3.45	0.5	0.1	49.4	56.0	8.5	13.9
Wed3-8	2834.45	BC	57.35	17.01	6.37	0.13	1.18	1.48	13.94	2.17	0.37	0.00		2.708	0.36	0.17	4.60	2.90	0.5	0.1	85.4	96.7	13.5	n.a. ^e
Wed3-9	2836.6	BC	56.02	19.49	13.34	0.00	2.72	0.90	6.68	0.65	0.20	0.00		2.711	1.10	0.19	8.46	4.86	0.5	0.1	76.2	85.2	11.5	17.4
Wed3-11b	2839.4	PL	51.83	16.02	18.37	0.08	8.55	3.52	1.05	0.11	0.47	0.00		2.740	0.02	4.00	0.85	0.09						
Wed3-10	2840.1	PL	43.01	15.17	30.27	0.10	4.41	5.78	0.48	0.22	0.56	0.00		2.763	0.02	2.90	1.30	0.07	0.5	0.1	56.5	58.7	12.6	13.5
Wed3-11	2841.9	SF	51.22	13.45	16.60	0.00	7.52	0.23	9.43	1.47	0.08	0.00		2.714	0.002	1.51	0.33	0.09						

(continued on next page)

Table 1 (continued)

Sample ID	Depth [m]	Depositional environment ^b	Mineralogy											Petrophysics ^a				Geomechanics										
			Quartz [mass-%]	Feldspar [mass-%]	Clay + Mica [mass-%]	Calcite [mass-%]	Dolomite [mass-%]	Siderite [mass-%]	Anhydrite [mass-%]	Gypsum [mass-%]	Barite [mass-%]	Hematite [mass-%]	Anatase [mass-%]	Density [g/cm ³]	Horizontal permeability [mD]	Vertical permeability [mD]	Horizontal porosity [%]	Vertical porosity [%]	Confining pressure P_c [MPa]	Pore fluid pressure P_p [MPa]	Yield stress σ_y [MPa]	Peak stress $(\sigma_1 - \sigma_3)_{\max}$ [MPa]	Apparent Young's Modulus E_a [GPa]	Apparent bulk Modulus K_a [GPa]				
Wed3-12 coarse ^c	2844.0	SF	45.64	16.44	24.42	0.00	3.92	9.19	0.21	0.11	0.00	0.07	2.727	0.05	0.01	0.95	1.04											
Wed3-12 ^c	2844.2	PL	34.73	13.64	45.07	0.00	5.53	0.11	0.56	0.10	0.00	0.24																
Wed3-13	2845.0																						5.0	-	179.7	196.1	26.0	22.2
Wed3-14	2845.0																						25.0	-	239.3	282.8	33.3	27.5
Wed3-15	2845.0																						50.0	-	261.5	378.3	30.9	25.8

^a Note that horizontal porosity and permeability are measured parallel to bedding, while vertical porosity and permeability are measured perpendicular to bedding.

^b PL = playa lake facies; SF = sheetflood facies; BC = braidchannel facies.

^c These samples had clear mineralogical zones, which were analysed separately. Transport properties were determined for whole plug samples.

^d The sample could not be brought to failure due to technical issues. Only elastic parameters could be determined from the elastic behaviour.

^e The apparent bulk modulus could not be calculated as the volumetric data was too strongly affected by temperature fluctuations.

itive ($a-b$)-value means the material is velocity-strengthening and will slip a-seismically, while for a negative ($a-b$)-value the material is said to be velocity-weakening and could potentially, though not necessarily, slip seismically (for a detailed explanation of RSF theory see Section 1.3 of the Supplementary Material; Dieterich, 1979; Ruina, 1983).

4. Results

4.1. Mineralogical and petrophysical analyses – unreacted vs. CO₂-exposed

The two WED-wells can be subdivided into three lithofacies: 1) braidchannel deposits consisting of the coarsest, sandy intervals; 2) sheetflood deposits consisting of fine- to medium-grained sandstones and siltstones; and 3) playa-lake deposits consisting of silty claystone. We will shortly describe the mineralogical composition of both wells below (see Table 1 and Fig. 2).

Though detrital compositions vary significantly between the three different depositional settings, no substantial differences in detrital compositions are observed between the two wells, (Table 1 and Fig. 2). The quartz content ranges between 11 and 77 mass-%, with playa-lake deposits having the lowest quartz contents and braided channel sandstones the highest. Samples with the lowest quartz content contain the highest clay content, with a total clay-micas content varying between 4 and 74 mass-% throughout the reservoirs (Table 1). Furthermore, WED3 contains significantly more feldspar than WED2, particularly K-feldspar (mainly microcline, minor amounts of orthoclase – cf. Fig. 2A and B, and Table 1). The anhydrite content is highest in braidplain and sheetflood sandstones (Fig. 2C and D). The total carbonate content is variable among the different samples (1–45 mass-%, dolomite is dominant – Fig. 2E), though no significant differences were seen between the two wells. Hematite content in WED2 is up to 5 mass-%, while WED3 is practically devoid of hematite.

In more detail, quartz grains are mostly monocrystalline, while micas are mainly muscovite, often aligned along the bedding planes. Carbonate clasts, as well as other framework grains, are often rimmed by clay minerals (Fig. 2B). In coarse-grained, braid-channel sandstones, syntaxial K-feldspar overgrowths are widely present, while they are less well-developed in playa-lake sediments. CO₂-exposed sandstones show more extensive pseudomorphic K-feldspar replacement than the unreacted material. In both wells, feldspar grains and authigenic cement are frequently partly dissolved, with the resulting secondary porosity being nearly always open (Fig. 2A and B). Macropores resulting from feldspar alteration are the main secondary porosity observed in WED2 (see Fig. 2A). Similar features are also seen in WED3, but mostly in the form of intragranular micro- and macropores in feldspar grains. Though bitumen is found in both wells, bitumen-staining was more prevalent in the CO₂-well (Fig. 2B). When bitumen coatings are present, open grain-dissolution secondary macropores often contain small relicts of feldspar grains. Large quartz overgrowths are observed in such bitumen-stained samples, with the overgrowths often trapping some of the bitumen, implying authigenic quartz growth occurred during oil-charging. Other authigenic cements, both pore-filling and pore-lining, consist of anhydrite (Fig. 2C and D), carbonates (dolomite–ankerite, 1–45 mass-%; minor amounts of siderite – see Fig. 2E) and barite (max. 0.2 mass-% in WED2; up to 2.5 mass-% in WED3).

Some of the coarse-grained sandstone beds in WED3 (e.g. samples WED3-3 and WED3-5; depth ~2821–2830 m – see Fig. 2E, F) have strikingly high porosities and permeabilities. These samples have low anhydrite contents, contain traces of calcite (<0.5 mass-% – see Table 1) and show indications of localised cement dissolution. The dissolved cement is interpreted to have been nodu-

lar, pre-compactional framework grain-replacive anhydrite. This cement was observed in nodules in coarser sandstones from both wells, where it extensively replaces mostly quartz grains. Its pre-compactional genesis is evident from the preserved large primary porosity and the un-evolved grain contacts in the cemented zones. Though the cement is clearly grain-replacive, original grain outlines could often be recognised in the cement texture. The zones in the CO₂-altered samples of WED3 where the anhydrite cement was dissolved are recognised from their excessive primary porosity and ragged quartz grain surfaces. The presence of dolomite–ankerite crystals in the highly porous zones confirms that the dissolved cement was not a carbonate.

Though CO₂-exposure did not seem to lead to drastic mineralogical difference between wells WED2 and WED3, markedly different porosity-permeability relationships were found for the unreacted and exposed material. The CO₂-exposed material (WED3) showed a stronger dependence of permeability on porosity (see also Table 1), attributed to the differences in diagenetic history before CO₂ emplacement. Due to the differences in structural setting, diagenesis in WED2 took place in an open chemical system, while WED3 was a closed system. Scarce bitumen remnants in WED2 attest to migration of hydrocarbon-bearing fluids through the reservoir, which explains the observed feldspar leaching. Hydrocarbon emplacement in WED3 is interpreted to have led to chemical isolation and consequent closed-system diagenesis. The presence of oil locally resulted in bleaching and carbonate cementation.

4.2. Mechanical strength and elastic parameters

For the **dry (room humidity) experiments** ($P_c^{\text{eff}} = 2\text{--}50$ MPa), the differential stress and volumetric strain versus axial strain curves show quasi-elastic loading behaviour, followed by yielding and failure at peak stress (Fig. 3 – solid curves). Overall, peak stress increases with P_c and the CO₂-exposed samples appear to be stronger than the unreacted material (cf. Fig. 3A and B), with the exception of the more porous zone in WED3, which is clearly weaker (Fig. 3C). Failure is characterised by a stress drop, directly followed by a rapid (apparent) increase in axial and volumetric strain due to the sudden release of elastic energy from the deformation apparatus. A pressure-dependent residual strength is attained by 1.9–4.6% axial strain. Over the entire confining pressure range, the volume data show net compaction, though after yielding dilatation (positive-going volume change) is observed (see Fig. 3D–F). After failure, dilatant volumetric strain is seen for the samples deformed at low P_c (≤ 5 MPa). All samples show brittle failure along either a single macroscopic fracture, or a conjugate set of two fractures, with the failure plane at $\sim 30^\circ$ to the σ_1 -direction.

Apparent Young's modulus increases roughly with confining pressure, with slightly lower values for the unreacted material (28.2 GPa at 50 MPa P_c) than for the CO₂-exposed samples (30.9 GPa at 50 MPa P_c). A similar trend is observed for the K_a -values (WED2: $K_a = 22.9$ GPa; WED3: $K_a = 25.8$ GPa, at 50 MPa P_c – Table 1).

The **wet (fully saturated) experiments** ($P_c^{\text{eff}} = 0.4\text{--}25$ MPa with $P_p = 0.1\text{--}0.5\text{--}10$ MPa) show mechanical behaviour very similar to the dry experiments ($P_p = 0.5\text{--}10$ MPa see Fig. 3; $P_p = 0.1$ MPa see Fig. 4). Furthermore, E_a - and K_a -values fall within the same order of magnitude as measured for dry material (Table 1). Note that for the near-unconfined, wet experiments ($P_c = 0.5$ MPa; $P_p = 0.1$ MPa), peak strength varies from 56.0 to 96.7 MPa (sample variability ± 16 MPa – see Fig. 4), with no clear dependence on the degree of CO₂-alteration. For these experiments, E_a and K_a are significantly lower than for the confined samples, measuring 8.2–14.8 GPa and 9.5–17.5 GPa, respectively.

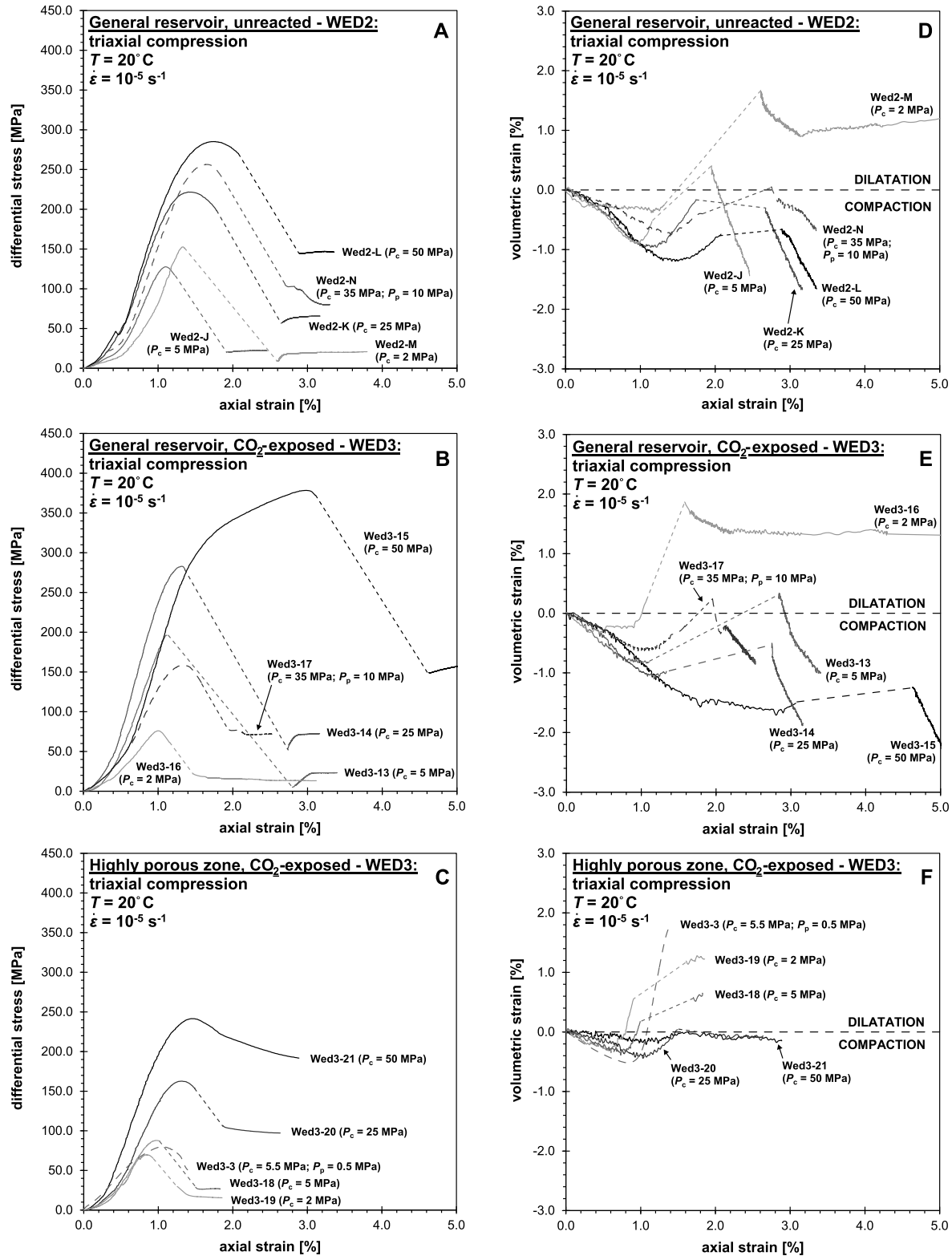


Fig. 3. Differential stress vs. axial strain (A–C) and volumetric strain vs. axial strain (D–F) for unreacted Röt Fringe Sandstone (A and D – WED2), CO₂-exposed Röt Fringe material taken from the general reservoir formation (B and E – WED3) and from the CO₂-exposed, highly porous zone (C and F – WED3). All experiments were performed at room temperature, at a strain rate of $\sim 10^{-5} \text{ s}^{-1}$, either under dry conditions (solid curves), or wet conditions (dashed curves). Where changes were too rapid to measure, differential stress and volumetric strain versus axial strain behaviour are interpolated linearly (dotted lines).

4.3. Frictional properties and velocity-dependence

For the **direct-shear experiments**, sliding friction coefficient versus shear displacement curves (Fig. 5A) mainly show strain-

hardening behaviour, with the exception of experiments on WED2 at $\sigma_n = 50 \text{ MPa}$, and on WED3 at $\sigma_n = 25 \text{ MPa}$. At low normal stress ($\sigma_n = 5 \text{ MPa}$), μ^* -values are relatively high ($\mu^* = 0.7\text{--}1.1$), while for higher normal stresses ($\sigma_n = 25\text{--}90 \text{ MPa}$)

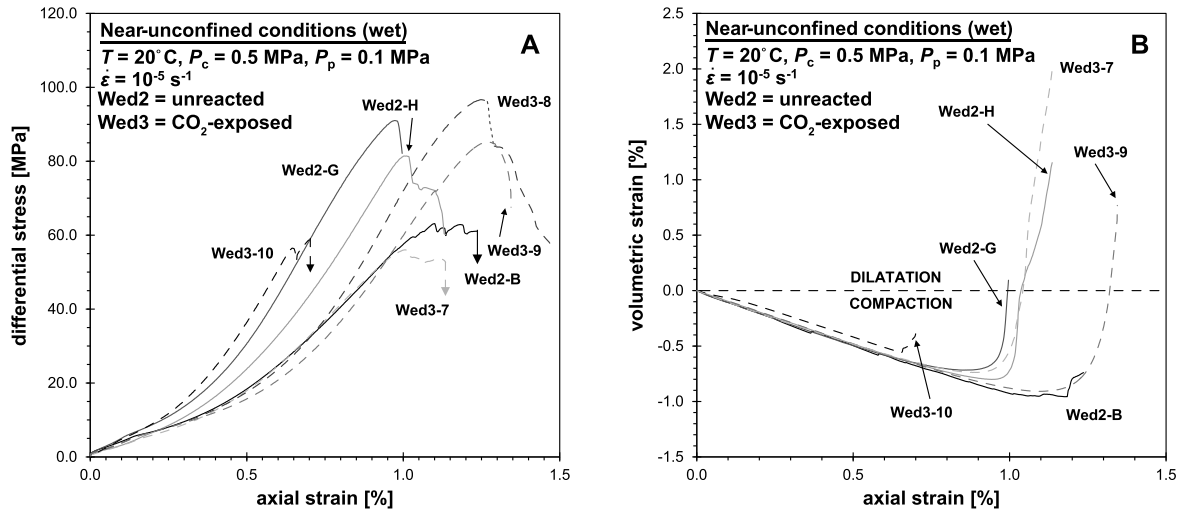


Fig. 4. A) Differential stress vs. axial strain, and B) volumetric strain vs. axial strain for near-unconfined experiments on wet Röt Fringe Sandstone (WED2 and WED3), deformed at room temperature, at a strain rate of $\sim 10^{-5}\text{ s}^{-1}$ at a $P_c = 0.5\text{ MPa}$ and $P_p = 0.1\text{ MPa}$.

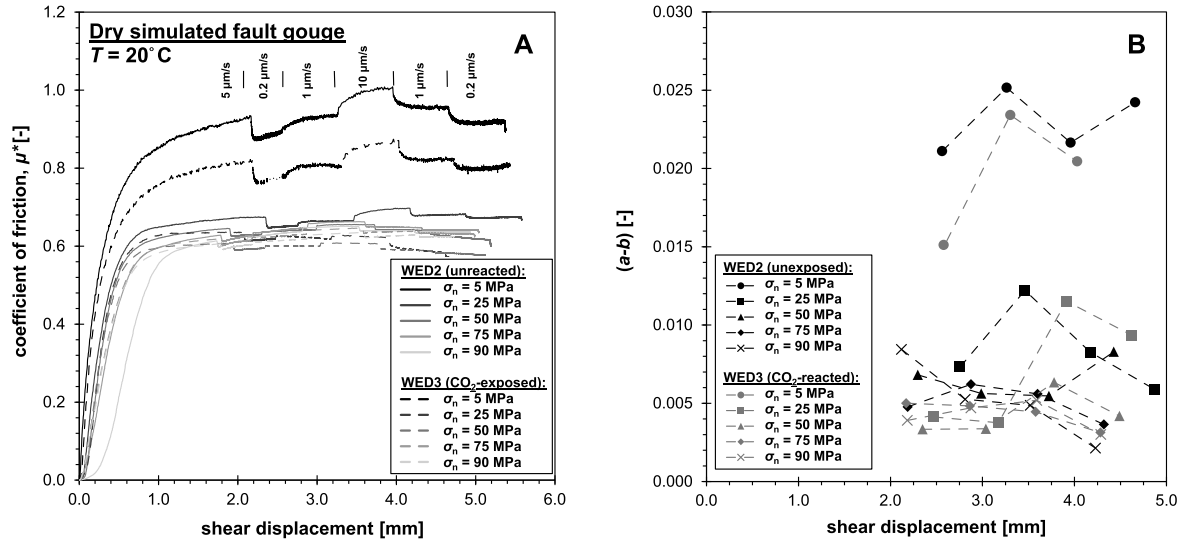


Fig. 5. A) Coefficient of friction, and B) $(a-b)$ -values vs. shear displacement for direct shear experiments on dry Röt Fringe Sandstone simulated fault gouges, performed at room temperature. Note that in A) the shear velocities are indicated at the top.

the steady-state friction coefficient varies between 0.5 and 0.7. Overall, WED2-gouges display slightly higher μ^* -values than WED3-gouges.

Using RSF-theory, the velocity-dependence of the individual velocity steps is expressed in terms of $(a-b)$ -values and plotted as a function of shear displacement (Fig. 5B). On the whole, $(a-b)$ -values are positive, reflecting stable sliding behaviour, with no significant difference between unreacted ($(a-b) = 0.0021\text{--}0.025$) and CO_2 -exposed fault gouge ($(a-b) = 0.0025\text{--}0.023$), and no clear trend with shear displacement. Note that, at low normal stress ($\sigma_n = 5\text{ MPa}$), $(a-b)$ -values are significantly higher than at higher σ_n , similar to the behaviour seen for the steady-state friction coefficient.

5. Chemical–mechanical effects of CO_2 /brine/rock interactions on rock properties

5.1. Petrophysical alterations induced by CO_2 -exposure

Long-term exposure to CO_2 -rich fluids did not result in overall drastic alteration of the Röt Fringe Sandstone reservoir rock. Substantial differences in porosity were observed only in mm-sized

zones in specific horizons. This specific impact of CO_2 /brine/rock interactions in the Werkendam reservoir is mainly attributed to a primary, sedimentological control on the distribution of reactive mineral phases in the reservoir. The finer grained, playa-lake and sheetflood sand/siltstones making up the Röt Formation contain considerably more carbonate and anhydrite cements, which are prone to CO_2 -induced alteration, but also have lower porosities and permeabilities. Reactive CO_2 -rich fluids entering those zones reach saturation with respect to anhydrite and carbonates before substantial alteration can occur, because of the lower water:rock ratios and the restricted flow through such beds compared to coarser, i.e. more permeable, horizons.

On the reservoir-scale, the CO_2 -rich brine is considered to have been channelled through the coarser, more permeable braid channel sandstone beds. The higher porosity of these beds resulted in a considerably higher water:rock ratio. Additionally, reactive cements are present in markedly smaller amounts, which reduces the fluid-buffering capacity of the rock, and consequently led to a higher relative impact of CO_2 -induced alteration. Anhydrite cement was mainly present as randomly distributed mm-sized nodules filling abundant primary porosity. Dissolution of these nodules resulted

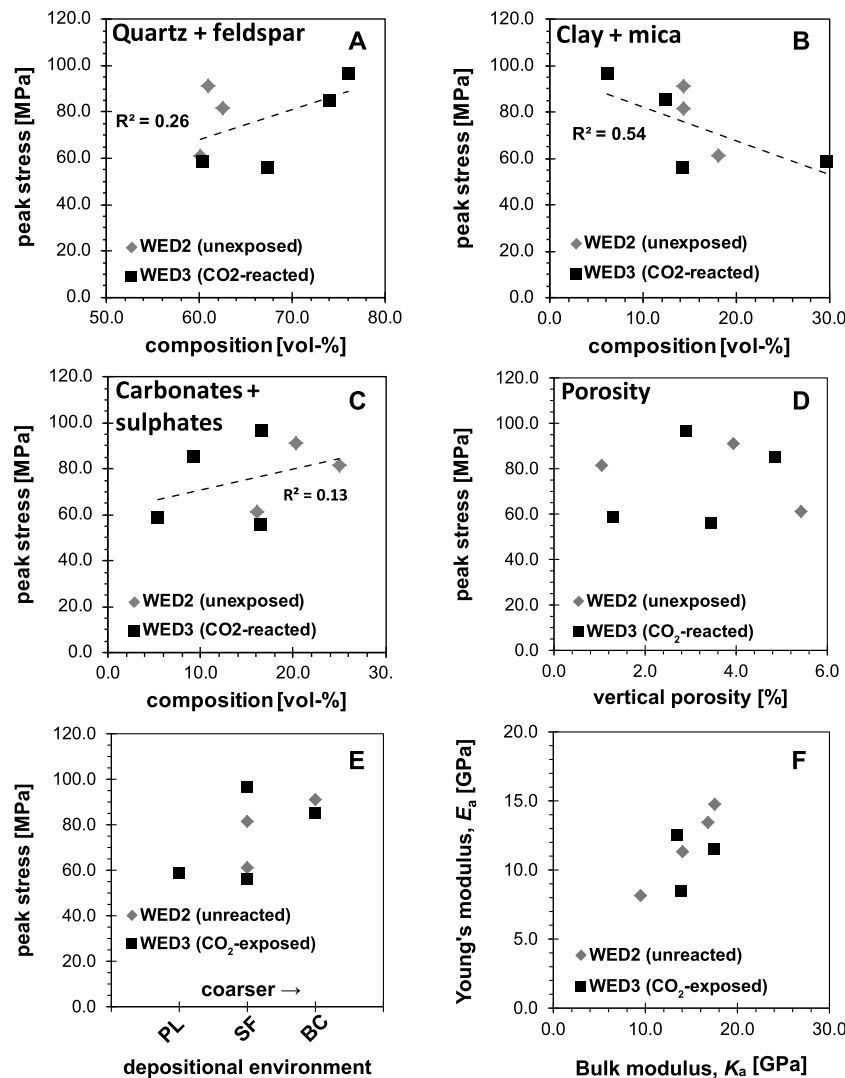


Fig. 6. Peak stress vs. rock composition, for A) quartz + feldspar, B) clay + mica, and C) carbonates + sulphates, D) vertical porosity (i.e. \perp to bedding), and E) depositional environment (i.e. 'grain size'); BC = braidchannel facies, SF = sheetflood facies, and PL = playa-lake facies. F) Apparent Young's modulus vs. apparent bulk modulus. Note that all experiments were performed under the same conditions (wet, near-unconfined: $P_c = 0.5$ MPa and $P_p = 0.1$ MPa), which warrants this comparison.

in substantial, but spatially very restricted alteration of the reservoir.

Besides the primary control on the distribution of reactive mineral phases, also the presence of oil in the Werkendam reservoir, prior to CO₂ charging, is considered to have limited the impact of CO₂-induced alteration. The sandstones exhibiting anhydrite dissolution contain euhedral dolomite–ankerite cements that show no substantial signs of dissolution, though dolomite–ankerite is generally considered to be reactive when in contact with CO₂-rich fluids. These crystals are rimmed by pyrobitumen, which is considered to have shielded them from dissolution by CO₂-exposure. Such bitumen coatings were not observed coating anhydrite, which can be attributed to the differences in surface charge between these minerals at typical reservoir pH, which control the relative wetting of their surfaces (Ney, 1973).

5.2. Effect of CO₂/brine/rock interactions on strength, frictional and elastic parameters

As mechanical behaviour is closely related to the petrophysical properties of the material, we investigated whether CO₂-exposure, and specifically any differences or changes in rock texture due to CO₂-exposure, affected the strength and elastic parameters of the

material (cf. Fig. 3A and B). In general, rock strength increases with increasing content of 'strong/hard minerals' (e.g. quartz, feldspar), and decreases with increasing amounts of 'weak/soft minerals' (e.g. clay, mica) and porosity (Lindqvist et al., 2007; Vernik et al., 1993). Therefore, we plotted the peak strength of experiments performed under the same conditions (i.e. the near-unconfined tests) against rock texture (mineralogy, porosity, depositional environment – see Fig. 6). It can be seen that strength generally does not correlate well with composition, nor with porosity (Fig. 6A, B and D). Only the total clay+mica content shows a weak negative correlation with peak strength ($R^2 = 0.54$ – see Fig. 6B). The depositional environment can be taken as a rough measure for grain size, and peak strength appears to roughly increase with grain size (Fig. 6E). These 'coarser' samples have a lower clay+mica content, i.e. less 'weak minerals', which might explain this trend (see Table 1). As expected, the elastic parameters, apparent Young's modulus and bulk modulus, correlate well (Jaeger et al., 2007), though no clear distinction can be made between the unreacted and CO₂-exposed materials (Fig. 6F). The lack of a simple correlation between rock texture parameters and rock strength suggests that for the Röt Fringe Sandstone strength depends on a more complex interplay between rock composition and porosity, most likely also depending on grain-to-grain contact structure (e.g. see Ulusay et al., 1994).

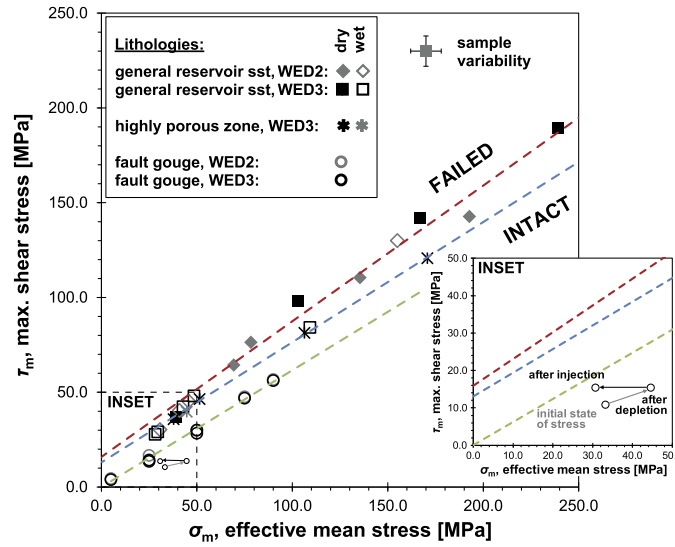


Fig. 7. Mohr–Coulomb failure envelopes, delineated in mean stress vs. maximum shear stress space, summarising the failure behaviour observed for rock samples obtained from the general reservoir, as well as from the more porous zones identified in WED3. In addition, the failure envelope for dry simulated fault gouge is also plotted. The inset shows the stress path a hypothetical field will follow upon gas/oil depletion and CO₂-injection.

Overall, though initially CO₂-exposed (WED3) sandstone appeared to be slightly stronger than unreacted material (WED2 – cf. Fig. 3), no clear distinction can be made between the mechanical behaviour of the larger parts of the two reservoirs when taking into account sample variability (± 16 MPa). Therefore, we conclude that for the Werkendam natural CO₂ field long-term exposure did not affect the strength of the larger parts of the reservoir and any general variations in strength were caused by local variations in diagenetic history. However, locally CO₂-exposure had a clear effect on mechanical properties, which needs to be quantified. This effect resulted from local variations in mineral quantity and distribution, and transport properties, affecting the local water:rock ratio controlling the extent of reaction, which in turn led to further, local changes in porosity.

To investigate the effect of chemical environment (dry, wet, CO₂-exposure) on strength, we employed the (modified) Mohr–Coulomb failure criterion to describe the peak failure data for all three rock types and the simulated fault gouges (Fig. 7). A failure criterion delineates the (effective) stress conditions under which the material is intact vs. has failed. As seen in Fig. 7, Mohr–Coulomb stress space is bounded by the maximum shear stress, $\tau_m = 1/2(\sigma_1 - \sigma_3)$, and the effective ‘two-dimensional’ mean stress, $\sigma_m = 1/2(\sigma_1 + \sigma_3) - P_p$. A linear fit through the data, i.e. the failure envelope, has the form $\tau_m = S_0 \cos \phi + \sigma_m \sin \phi$, where S_0 is the cohesion and ϕ is the angle of internal friction (Jaeger et al., 2007). Since CO₂-exposure did not significantly affect rock strength, data obtained for WED2 and WED3 are combined. The failure criteria for dry rock are given as,

General reservoir sandstone:

$$\tau_m = 0.7158\sigma_m + 15.871 \quad (R^2 = 0.9816) \quad (1)$$

Highly porous zone (WED3):

$$\tau_m = 0.6342\sigma_m + 12.994 \quad (R^2 = 0.9993) \quad (2)$$

Fault gouge: $\tau_m = 0.6186\sigma_m \quad (R^2 = 0.9949) \quad (3)$

From the dry failure envelopes, uniaxial compressive strength C_0 (i.e. rock strength at $P_c = 0$; $C_0 = 2S_0 \cos \phi / (1 - \sin \phi)$) and the internal coefficient of friction μ ($\mu = \tan \phi$) can be derived (Jaeger et al., 2007). For the general Werkendam reservoir $C_0 = 111.7$ MPa and $\mu = 1.03$, while by comparison the μ^* -value for fault gouge is similar at low σ_n ($\mu^* = 0.7$ – 1.1) but lower at $\sigma_n > 25$ MPa

($\mu^* = 0.5$ – 0.7). The strength of the more ‘porous’ zones is roughly one-third lower than that of the larger part of the reservoir ($C_0 = 16.8$ MPa, $S_0 = 71.0$ MPa and $\mu = 0.82$). Note that the internal coefficient of friction μ and the sliding coefficient of friction μ^* are not necessary equal as μ is involved with the formation of a new fracture, while μ^* describes motion on an existing plane. At low normal stress μ^* and μ are more comparable, most likely due to some degree of cohesion in the simulated fault gouge at low σ_n -values. Furthermore, looking at the cohesion values obtained for intact samples of the general reservoir ($S_0 = 22.7$ MPa) and the CO₂-exposed, highly porous zone ($S_0 = 16.8$ MPa) it’s seen that the latter shows lower S_0 -values. This can be the result of the higher porosity and/or caused by the dissolution of anhydrite cement, affecting the rock framework strength, though we cannot differentiate which process had a stronger influence.

In addition to the dry data, we plotted wet peak strength in Mohr–Coulomb stress space (open diamonds and squares in Fig. 7). If no water-weakening effects occur than experiments performed under the same effective stress conditions yield similar results, both for the general reservoir (i.e. Wed2-K vs. Wed2-N and Wed3-20 vs. Wed3-17) and the highly porous zones (Wed3-18 vs. Wed3-3). Within the range of sample variability the wet data fall in line with the failure envelopes outlined by the dry data. This means that the short-term (i.e. on the time-scale of lab experiments, hours–days) failure behaviour of the Röt Fringe Sandstone is controlled by the law of effective stress ($\sigma_i^{\text{eff}} = \sigma_i - P_p$) with no discernible chemical weakening effects. This means that the failure criterion for dry sandstone can be used to delineate the (effective) stress conditions under which intact reservoir rock will be intact versus failed, with or without pore fluid.

5.3. Implications for the CO₂-storage system and long-term integrity predictions

Numerous natural CO₂ accumulations can be found globally, each with varying degrees of fluid–rock interaction in response to long-term CO₂-exposure, though only few of these sites have been studied in detail. In the presence of reactive minerals, such as Fe-rich volcanic fragments and chlorite (Ladbroke Grove, Otway, Australia), widespread precipitation of ankerite and Fe-rich carbonates is observed (Bickle et al., 2013; Higgs et al., 2015). In contrast, in fields with limited availability of Ca²⁺ and Mg²⁺ (e.g. Fizzy gas

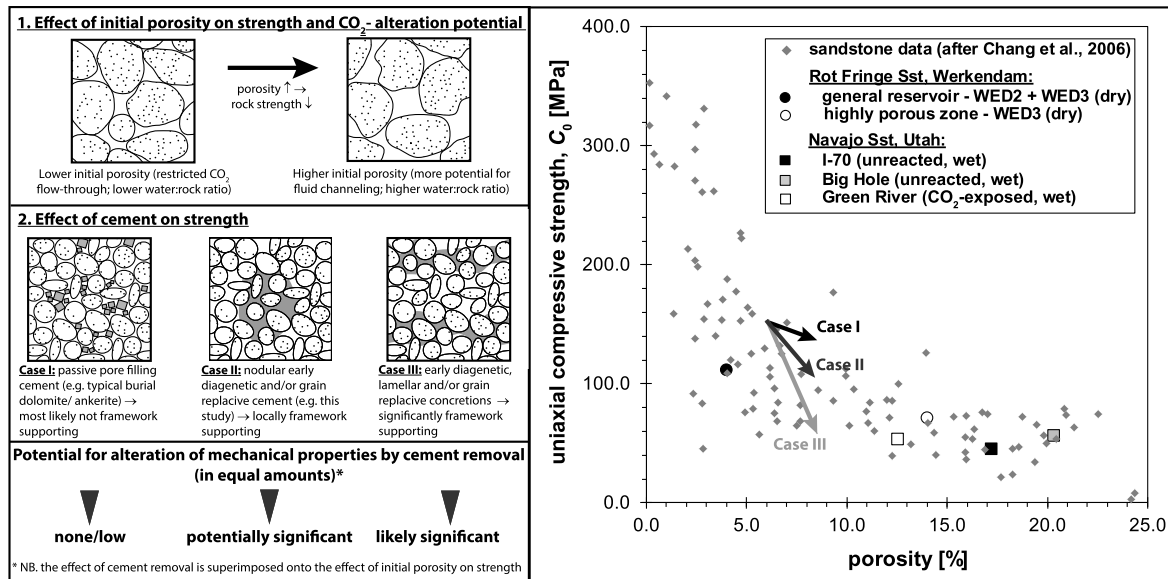


Fig. 8. Schematic diagram illustrating the effect of initial porosity (top left) and cement (bottom left) have on rock strength, as well as on the potential for CO₂-alteration. The graph on the right shows the dependence of C_0 on porosity for a range of different sandstones (data from Chang et al., 2006). We illustrated the potential effect cement removal due to CO₂-exposure can have on rock strength for each of the three different cases of cement distribution. The C_0 -data obtained for sandstones from two natural analogue fields, the Röt Fringe Sandstone (this study) and Navajo Sandstone (Busch et al., 2014), are shown as well.

field, Southern North Sea) little reaction is observed (Bickle et al., 2013; Heinemann et al., 2013). Obviously, such marked differences in chemical response already make comparison between different analogue fields difficult. Therefore, we will not attempt such a comparison, as the Werkendam natural CO₂ analogue poses a rather unique case study. In fact, the presence of bitumen coatings makes our findings also highly suitable for assessing and understanding the evolution of enhanced oil recovery (EOR) projects.

Our study suggests that the long-term impact of CO₂-induced alteration on the mechanical properties of sandstone reservoirs tends to be restricted to specific lithotypes. The CO₂-alteration potential of sandstones is mainly controlled by the rock-buffering capacity provided by reactive minerals such as carbonates and Ca-sulphates, and by the amount of water each volume of rock is exposed to. The latter is determined by the porosity of the rock, and the flux of reactive fluid through it. Sandstones with low porosities and high reactive mineral contents are less prone to significant alteration than porous beds with low reactive mineral contents, because they are generally exposed to smaller amounts of fluid, and have abundant capacity to buffer reactive fluids. A further constraint is that the impact of CO₂-induced alteration on mechanical properties also depends on the distribution of the reactive minerals. When small amounts of cement are homogeneously distributed in the rock, dissolving them is likely to have a much smaller impact than when small amounts of reactive minerals are concentrated at specific locations, i.e. where they locally make up a substantial part of the rock volume. In addition, dissolution of early diagenetic, i.e. pre-compactional, or framework grain-replacive cements, is likely to have a more substantial impact on mechanical properties because such cements support the framework of the rock.

Failure strength of sandstones (confined and unconfined) is in part controlled by porosity (Chang et al., 2006; Vernik et al., 1993; Wong and Baud, 2012), though the effect of framework-supporting cement and grain-to-grain contact structure cannot be ignored (e.g. Ulusay et al., 1994). For sandstones with the same, or similar, composition, a difference in (initial) porosity of ~10% will usually be associated with a significant difference in failure strength (see C_0 -porosity plot in Fig. 8). At the same time, the anhydrite cement observed in the porous zones in this study is in part (lo-

cally) supporting the framework grains, so even a few % removal of this cement must also contribute to a weakening effect (compare cases I–III and arrows in C_0 -porosity plot in Fig. 8). However, we cannot quantify the relative importance of the effect without further work, e.g. studying samples with anhydrite nodules with higher initial porosities, similar to those seen in WED3 (case II in Fig. 8), before and after CO₂-exposure. At the reservoir scale, such quantification would require testing of a very large number of samples, which is currently not feasible.

These observations regarding the impact of reactivity and water:rock ratio on mechanical properties, are in line with the results from a chemo-mechanical study performed on the Green River natural CO₂ field, Utah, USA (Busch et al., 2014). Preliminary results for the Navajo Sandstone showed slight differences in rock strength between the unreacted and CO₂-exposed material. It was concluded that these differences mainly resulted from lateral variations in depositional environment and burial history, and not from CO₂-alteration given the very low reactivity of the host rock. Overall, both natural CO₂ analogue sandstone studies suggest that only in case of substantial dissolution of framework grains or framework-supporting cements significant changes in the mechanical behaviour are to be expected. Therefore, for assessment of potential CCS or EOR sites, the reservoir should not only be screened for its overall grain reactivity and porosity (i.e. fluid buffering capacity), but also for its overall vs. local porosity (i.e. water:rock ratio, fluid channeling potential), and cement content and distribution (case I is preferential over cases II and III, Fig. 8).

Studies on the frictional behaviour of simulated fault gouges have shown that ductile minerals, such as carbonates and sulphates, could potentially lead to velocity-weakening behaviour, especially at temperatures >80–120 °C (Pluymakers et al., 2014; Scuderi et al., 2013; Verberne et al., 2014). Other typical minerals, such as quartz and clays, generally do not show velocity-weakening behaviour, not even under wet conditions (e.g. Ikari et al., 2007). Since the presence of CO₂ itself does not seem to affect fault friction (Samuelson and Spiers, 2012), it is inferred that the frictional behaviour of faults is mainly controlled by their mineralogy, as well as fault heterogeneity (Tesei et al., 2014). In general, the potential for induced seismicity seems to hinge on the presence of ductile minerals. Therefore, it's important to understand

their relative proportions compared to other minerals in faults when assessing a potential CCS site.

To assess the likelihood of reservoir failure and fault reactivation as a result of hydrocarbon production, as well as CO₂ injection, we performed simple stress path calculations (Fig. 7, see inset). It was assumed that the reservoir is isotropic and of infinite lateral extent, i.e. no deformation in the horizontal direction (Hettema et al., 1998; Soltanzadeh and Hawkes, 2008). The stress regime is taken to be extensional (Heidbach et al., 2008), i.e. $\sigma_v = \sigma_1$ and $\sigma_h = \sigma_2 = \sigma_3 = 0.67\sigma_v$. The initial vertical stress σ_v is taken to be equal to the overburden pressure, meaning $\sigma_v = 66$ MPa at a depth of 2880 m, assuming an overburden density of 2300 kg/m³. The initial pore pressure in the field is 20.9 MPa, i.e. below hydrostatic pressure. Knowing the elastic behaviour of the reservoir (see Table 1), the normalised stress arching ratios are given as $\gamma_v = 0$ and $\gamma_h = \frac{(1-2\nu)}{(1-\nu)} = 0.57$ for Poisson's ratio $\nu = (3K_a - E_a)/6K_a = 0.30$ (Soltanzadeh and Hawkes, 2008). The change in effective stress, caused by changes in pore pressure during depletion, can be calculated using $\Delta\sigma'_i = -(1 - \gamma_i)\alpha\Delta P$, where $i = v, h$ and α is Biot's coefficient (taken to be 1) (Soltanzadeh and Hawkes, 2008). During re-pressurisation, it is assumed that the reservoir stress path is irreversible, i.e. $\gamma_v = \gamma_h = 0$, as is commonly observed for reservoirs (Santarelli et al., 1998).

In Fig. 7 (see also the inset), we plotted the failure envelopes (Eqs. (1)–(3)), together with the initial state of stress within the reservoir. Pore pressure depletion from 20.9 MPa to 5 MPa results in an increase in mean stress and maximum shear stress, though the state of stress remains away from the failure envelopes, as well as from the fault reactivation line. Upon re-pressurisation due to CO₂ injection, the pore pressure is increased to 90% of the original reservoir pressure ($P_{CO_2} = 18.8$ MPa). Though the state of stress moves towards lower mean stress values, no failure of the general reservoir or of the highly porous zones, nor fault slip, is expected. For fault slip to occur, γ_h would have to be ~ 0.8 , i.e. $\nu = 0.17$, which is an unrealistically low Poisson's ratio value for sandstone. However, even if fault reactivation would occur, the $(a-b)$ -values determined for the Röt Fringe Sandstone are positive, suggesting stable slip will occur, making induced seismicity unlikely.

6. Conclusions

We performed petrophysical analysis and geomechanical experiments on samples obtained from the sandstone reservoir of a natural CO₂ field (WED3) and its unreacted counterpart (WED2 – Röt Fringe Sandstone, Werkendam field, the Netherlands). Our aim was to study the chemical–hydro-mechanical coupling for the selected rock material, prior and after long-term CO₂-exposure.

- Overall, the unreacted and CO₂-exposed Röt Fringe Sandstone show relatively small differences in mineralogy, with the CO₂-exposed well showing some dissolution of hematite, precipitation of calcite and higher feldspar contents resulting in slightly higher porosity and permeability. Furthermore, bitumen coatings locally protected specific minerals from CO₂/brine/rock interactions. Specific zones within WED3 (CO₂-exposed) show significant dissolution of nodular anhydrite, which locally (on a mm-scale) resulted in a significant increase in porosity and permeability.
- The mechanical behaviour of the dry, unreacted and CO₂-exposed sandstone ($P_c^{\text{eff}} = 2\text{--}50$ MPa) shows an increase in peak stress with increasing confining pressure. Peak strength variations caused by sample variability are ± 16 MPa. From experiments performed under the same conditions, it is shown that the mechanical behaviour of the sandstone is a complex interplay between rock composition, texture and porosity.

- The chemical environment (dry vs. wet) did not affect the short-term (hours–days) mechanical behaviour. The failure behaviour of dry and wet Röt Fringe Sandstone can be described by a Mohr–Coulomb failure envelope: $\tau_m = 0.7158\sigma_m + 15.871$. In addition, more ‘porous’ zones, formed by CO₂-induced anhydrite dissolution, are described as: $\tau_m = 0.6342\sigma_m + 12.994$. These are significantly weaker than the bulk of the reservoir due to their higher porosity and/or removal of anhydrite cement.
- The frictional behaviour of simulated fault gouge, prepared from unreacted and CO₂-exposed sandstone, shows friction coefficients of $\sim 0.5\text{--}0.7$. Under all conditions ($\sigma_n = 5\text{--}90$ MPa), the gouges show velocity-strengthening behaviour, meaning stable sliding upon slip acceleration.
- In general, for mechanical modelling purposes, mechanical parameters obtained for unreacted (pre-CO₂ injection) rock can be used to evaluate the long-term mechanical behaviour of the reservoir, unless CO₂-induced reactions will lead to dissolution of framework supporting grains or cements.
- CO₂-induced chemical changes may result in significant mechanical weakening in porous and permeable sandstones with overall relatively small amounts of reactive minerals. This is the case when reactive minerals are locally concentrated as early diagenetic, precompactional and/or framework-replacive nodular, framework supporting cements. In theory this may affect the long-term mechanical integrity of the storage site. It is therefore recommended to screen potential storage sites for such cements.
- Stress path and fault reactivation calculations show that failure of the larger reservoir and/or the CO₂-altered zones, and fault reactivation are unlikely under realistic depletion and injection conditions. If fault reactivation does occur, it will be in a stable manner, meaning no induced seismicity is expected.

Acknowledgements

This research has been carried out in the context of the CATO-2-program. CATO-2 is the Dutch national research program on CO₂ Capture and Storage technology (CCS). The program is financially supported by the Dutch government (Ministry of Economic Affairs) and the CATO-2 consortium parties. We thank Nederlandse Aardolie Maatschappij (NAM) for providing samples and data and NAM and Shell Global Solutions for the allowance to publish this study. EB and PB thank Shell Global Solutions for providing funding for their research. Finally we thank Dr. Brett Carpenter and two anonymous reviewers for constructive and useful comments that helped improving the quality of this paper.

Appendix A. Supplementary material

Supplementary material related to this article can be found online at <http://dx.doi.org/10.1016/j.epsl.2015.07.044>.

References

- Baines, S.J., Worden, R.H., 2004. The long-term fate of CO₂ in the subsurface: natural analogues for CO₂ storage. *Geol. Soc. (Lond.) Spec. Publ.* 233, 59–85.
- Baud, P., Schubnel, A., Wong, T.-F., 2000. Dilatancy, compaction, and failure mode in Solnhofen limestone. *J. Geophys. Res.* 105, 19289–19303.
- Bickle, M., Kampman, N., Wigley, M., 2013. Natural analogues. *Rev. Mineral. Geochem.* 77, 15–71.
- Burnside, N.M., Shipton, Z.K., Dockrill, B., Ellam, R.M., 2013. Man-made versus natural CO₂ leakage: a 400 k.y. history of an analogue for engineered geological storage of CO₂. *Geology* 41, 471–474.
- Busch, A., Kampman, N., Hangx, S.J., Snippe, J., Bickle, M., Bertier, P., Chapman, H., Spiers, C.J., Pijnenburg, R., Samuelson, J., Evans, J.P., Maskell, A., Nicholl, J., Pipich, V., Di, Z., Rother, G., Schaller, M., 2014. The green river natural analogue as a field laboratory to study the long-term fate of CO₂ in the subsurface. *Energy Proc.* 63, 2821–2830.

- Chang, C., Zoback, M.D., Khaksar, A., 2006. Empirical relations between rock strength and physical properties in sedimentary rocks. *J. Pet. Sci. Eng.* 51, 223–237.
- Dieterich, J.H., 1979. Modeling of rock friction: 2. Simulation of preseismic slip. *J. Geophys. Res.* 84, 2169–2175.
- Dooley, J.J., Dahowski, R.T., Davidson, C.L., Wise, M.A., Gupta, N., Kim, S.H., Malone, E.L., 2006. Carbon dioxide capture and geologic storage – a core element of a global energy technology strategy to address climate change. In: *The Global Energy Technology Strategy Program*.
- Fredrich, J.T., Evans, B., Wong, T.-F., 1989. Micromechanics of the brittle to plastic transition in Carrara marble. *J. Geophys. Res.* 94, 4129–4145.
- Geluk, M.C., 2005. Stratigraphy and tectonics of Permo-Triassic basins in the Netherlands and surrounding areas. University of Utrecht, p. 171.
- Gilfillan, S.M.V., Lollar, B.S., Holland, G., Blagburn, D., Stevens, S., Schoell, M., Cassidy, M., Ding, Z., Zhou, Z., Lacrampe-Couloume, G., Ballentine, C.J., 2009. Solubility trapping in formation water as dominant CO₂ sink in natural gas fields. *Nature* 458, 614–618.
- Global Carbon Project, 2015. Global carbon budget 2014. <http://www.globalcarbonproject.org/carbonbudget/>. Accessed June 15th 2015.
- Hangx, S., van der Linden, A., Marcelis, F., Bauer, A., 2013. The effect of CO₂ on the mechanical properties of the Captain Sandstone: geological storage of CO₂ at the Goldeneye field (UK). *Int. J. Greenh. Gas Control* 19, 609–619.
- Hangx, S.J.T., Spiers, C.J., Peach, C.J., 2010a. Creep of simulated reservoir sands and coupled chemical–mechanical effects of CO₂ injection. *J. Geophys. Res.* 115, B09205.
- Hangx, S.J.T., Spiers, C.J., Peach, C.J., 2010b. Mechanical behavior of anhydrite caprock and implications for CO₂ sealing capacity. *J. Geophys. Res.* 115, B07402.
- Heidbach, O., Tingay, M., Barth, A., Reinecker, J., Kurfes, D., Müller, B., 2008. The World Stress Map database release 2008.
- Heinemann, N., Wilkinson, M., Haszeldine, R.S., Fallick, A.E., Pickup, G.E., 2013. CO₂ sequestration in a UK North Sea analogue for geological carbon storage. *Geology* 41, 411–414.
- Hetttema, M.H.H., Schutjens, P.M.T.M., Verboom, B.J.M., Gussinklo, H.J., 1998. Production-induced compaction of a sandstone reservoir: the strong influence of stress path. *SPE-65410-PA* 3, pp. 342–347.
- Higgs, K.E., Haese, R.R., Golding, S.D., Schacht, U., Watson, M.N., 2015. The Pretty Hill Formation as a natural analogue for CO₂ storage: an investigation of mineralogical and isotopic changes associated with sandstones exposed to low, intermediate and high CO₂ concentrations over geological time. *Chem. Geol.* 399, 36–64.
- IEA, 2013. Redrawing the energy-climate map: World energy outlook special report. International Energy Agency, p. 134.
- Ikari, M.J., Saffer, D.M., Marone, C., 2007. Effect of hydration state on the frictional properties of montmorillonite-based fault gouge. *J. Geophys. Res.* 112, B06423.
- IPCC, 2007. Climate change 2007: the physical science basis. In: Solomon, S., Qin, D., Manning, M., Marquis, M., Averyt, K., Tignor, M.M.B., Le Roy Miller, J.H., Chen, Z. (Eds.), *Contribution of Working Group I to the Fourth Assessment Report of the IPCC*. Cambridge University Press, Cambridge and New York.
- Jaeger, J.C., Cook, H.G.W., Zimmerman, R.W., 2007. *Fundamentals of Rock Mechanics*, 4th ed. Blackwell Publishing, Carlton, Australia.
- Kampman, N., Bickle, M., Wigley, M., Dubacq, B., 2014. Fluid flow and CO₂/fluid/mineral interactions during CO₂-storage in sedimentary basins. *Chem. Geol.* 369, 22–50.
- Lindqvist, J.E., Åkesson, U., Malaga, K., 2007. Microstructure and functional properties of rock materials. *Mater. Charact.* 58, 1183–1188.
- Major, J.R., Eichhubl, P., Dewers, T.A., Urquhart, A.S., Olson, J.E., Holder, J., 2014. The Effect of CO₂-Related Diagenesis on Geomechanical Failure Parameters: Fracture Testing of CO₂-Altered Reservoir and Seal Rocks from a Natural Analog at Crystal Geyser, Utah. American Rock Mechanics Association.
- Marbler, H., Erickson, K., Schmidt, M., Lempp, C., Pöhlmann, H., 2013. Geomechanical and geochemical effects on sandstones caused by the reaction with supercritical CO₂: an experimental approach to in situ conditions in deep geological reservoirs. *Environ. Earth Sci.* 69, 1981–1998.
- May, F., 2005. Alteration of wall rocks by CO₂-rich water ascending in fault zones: natural analogues for reactions induced by CO₂ migrating along faults in siliclastic reservoir and caprocks. *Oil Gas Sci. Technol.* 60, 19–32.
- Mikhailitsevich, V., Lebedev, M., Gurevich, B., 2014. Measurements of the elastic and anelastic properties of sandstone flooded with supercritical CO₂. *Geophys. Prospect.* 62, 1266–1277.
- Moore, J., Adams, M., Allis, R., Lutz, S., Rauzi, S., 2005. Mineralogical and geochemical consequences of the long-term presence of CO₂ in natural reservoirs: an example from the Springerville-St. Johns Field, Arizona, and New Mexico, U.S.A. *Chem. Geol.* 217, 365–385.
- Ney, P., 1973. *Zeta-Potentiale und Flotierbarkeit von Mineralien*. Springer-Verlag, Wien, New York.
- Paterson, M.S., Wong, T.-f., 2005. *Experimental Rock Deformation: The Brittle Field*, 2nd ed. Springer, Berlin.
- Pearce, J., Czernichowski-Lauriol, I., Lombardi, S., Brune, S., Nador, A., Baker, J., Pauwels, H., Hatzianannis, G., Beaubien, S., Faber, E., 2004. A review of natural CO₂ accumulations in Europe as analogues for geological sequestration. *Geol. Soc. (Lond.) Spec. Publ.* 233, 29–41.
- Pluymakers, A.M.H., Samuelson, J.E., Niemeijer, A.R., Spiers, C.J., 2014. Effects of temperature and CO₂ on the frictional behavior of simulated anhydrite fault rock. *J. Geophys. Res.*, Solid Earth 119, 2014JB011575.
- Racero-Baena, A., Drake, S.J., 1996. Structural style and reservoir development in the West Netherlands oil province. In: Rondeel, H.E., Batjes, D.A.J., Nieuwenhuijs, W.H. (Eds.), *Geology of Gas and Oil Under The Netherlands – Royal Geological and Mining Society of the Netherlands (KNGMG)*. Kluwer Academic Publishers, Dordrecht, pp. 211–227.
- Ruina, A., 1983. Slip instability and state variable friction laws. *J. Geophys. Res.* 88, 10359–10370.
- Samuelson, J., Spiers, C.J., 2012. Fault friction and slip stability not affected by CO₂ storage: evidence from short-term laboratory experiments on North Sea reservoir sandstones and caprocks. *Int. J. Greenh. Gas Control* 11S, S78–S90.
- Santarelli, F.J., Tronvoll, J.T., Svennekjaer, M., Skeie, H., Henriksen, R., Bratli, R.K., 1998. Reservoir stress path: the depletion and the rebound. In: *SPE/ISRM Eurock'98. Society of Petroleum Engineers, Trondheim, Norway (SPE/ISRM 47350)*.
- Scuderi, M.M., Niemeijer, A.R., Collettini, C., Marone, C., 2013. Frictional properties and slip stability of active faults within carbonate–evaporite sequences: the role of dolomite and anhydrite. *Earth Planet. Sci. Lett.* 369–370, 220–232.
- Soltanzadeh, H., Hawkes, C., 2008. Semi-analytical models for stress change and fault reactivation induced by reservoir production and injection. *J. Pet. Sci. Eng.* 60, 71–85.
- Streit, J.E., Watson, M.N., 2004. Estimating rates of potential CO₂ loss from geological storage sites for risk and uncertainty analysis. In: *7th International Conference on Greenhouse Gas Control Technologies*. Vancouver, Canada.
- Tesei, T., Collettini, C., Barchi, M.R., Carpenter, B.M., Di Stefano, G., 2014. Heterogeneous strength and fault zone complexity of carbonate-bearing thrusts with possible implications for seismicity. *Earth Planet. Sci. Lett.* 408, 307–318.
- Trippetta, F., Collettini, C., Barchi, M.R., Lupattelli, A., Mirabella, F., 2013. A multi-disciplinary study of a natural example of a CO₂ geological reservoir in central Italy. *Int. J. Greenh. Gas Control* 12, 72–83.
- Ulusay, R., Türeli, K., Ider, M.H., 1994. Prediction of engineering properties of a selected litharenite sandstone from its petrographic characteristics using correlation and multivariate statistical techniques. *Eng. Geol.* 38, 135–157.
- Verberne, B.A., Spiers, C.J., Niemeijer, A.R., De Bresser, J.H.P., De Winter, D.A.M., Plümpner, O., 2014. Frictional properties and microstructure of calcite-rich fault gouges sheared at sub-seismic sliding velocities. *Pure Appl. Geophys.* 171, 2617–2640.
- Verdon, J.P., Kendall, J.-M., Stork, A.L., Chadwick, R.A., White, D.J., Bissell, R.C., 2013. Comparison of geomechanical deformation induced by megatonne-scale CO₂ storage at Sleipner, Weyburn, and In Salah. *Proc. Natl. Acad. Sci. USA* 110, E2762–E2771.
- Vernik, L., Bruno, M., Bovberg, C., 1993. Empirical relations between compressive strength and porosity of siliciclastic rocks. *Int. J. Rock Mech. Min. Sci. Geomech. Abstr.* 30, 677–680.
- Watson, M.N., Zwingmann, N., Lemon, N.M., 2004. The Ladbroke Grove–Katnook carbon dioxide natural laboratory: a recent CO₂ accumulation in a lithic sandstone reservoir. *Energy* 29, 1457–1466.
- Wong, T.-f., Baud, P., 2012. The brittle-ductile transition in porous rock: a review. *J. Struct. Geol.* 44, 25–53.
- Zoback, M.D., Byerlee, J.D., 1975. The effect of cyclic differential stress on dilatancy in Westerly granite under uniaxial and triaxial conditions. *J. Geophys. Res.* 80, 1526–1530.